





Cite this: *RSC Appl. Interfaces*, 2024, **1**, 1265

# Investigation into the adhesion properties of PFAS on model surfaces†

Jack Welchert,<sup>a</sup> McKenna Dunmyer,<sup>b</sup> Lynn Carroll, <sup>b</sup> Irbis Martinez,<sup>b</sup> Trisha J. Lane,<sup>b</sup> Daniel A. Bellido-Aguilar,<sup>b</sup> Suchol Savagatrup<sup>b</sup> and Vasiliki Karanikola <sup>\*b</sup>

Perfluoroalkyl substances (PFAS) are a category of environmental contaminants of increasing global concern. Common treatments are adsorption, ion exchange and pressure-driven membrane processes, all of which are non-selective, demonstrate quick breakthrough, unsustainable regeneration, and require disposal of concentrates with high PFAS concentrations. The challenges presented by modern treatment practices to sustainably remove PFAS from water have led researchers to investigate alternative, economically viable PFAS remediation options such as development of novel sorbents. An integral step in developing novel PFAS removal matrices is material characterization; specifically pertaining to molecular interactions between adsorbent and adsorbate. To investigate this fundamental relationship, atomic force microscopy (AFM) was utilized to produce force profiles between two PFAS, perfluorooctanesulfonate (PFOS) and perfluorobutanesulfonate (PFBS), and surfaces in different conditions. Silicon wafers were surface modified with three silane molecules: aminopropyltriethoxysilane (APTES), triethoxy(octyl)silane, and trimethoxy(octadecyl)silane to observe the effect of surface polarity and hydrophobicity on PFAS adhesion. Force spectroscopy measurements taken with AFM were conducted in deionized water, sodium chloride, and magnesium chloride to examine the impact of ions on PFAS adhesion. The results of this study show that the force of PFAS adhesion onto surfaces is lowest in deionized water and increases in strength with addition of divalent cations.

Received 22nd June 2024,  
Accepted 9th July 2024

DOI: 10.1039/d4lf00228h

rsc.li/RSCApplInter

## 1. Introduction

Per and polyfluoroalkyl substances (PFAS) are a category of synthetic chemicals, widely used for commercial and industrial practices. Their application offers unparalleled physicochemical properties due to their aliphatic backbone being comprised of strong, and stable carbon-fluorine (C-F) bonds rather than conventional hydrocarbon bonds. PFAS molecules that possess fully fluorinated carbon chains tend to convey superior mechanical and thermal resistance in comparison to their alkyl homologs.<sup>1</sup> This renders PFAS useful for situations where robust chemical properties are required. In addition to their enduring qualities, PFAS present with greater hydrophobic and oleophobic behavior, as well as corrosion resistance, than their alkyl counterparts due to tighter steric structuring and larger molecular geometry.<sup>2</sup> The

forementioned properties render PFAS to be highly functionable and stable molecules. Conversely, PFAS remain as one of the biggest environmental challenges in relation to their widespread contamination and detection in global water supplies. The increased molar volume and bond strength of PFAS protect the fluorocarbon backbone from both natural and biological degradation pathways, allowing them to accumulate in the environment and transport into water supplies. The most common group of PFAS utilized are perfluoroalkyl acids (PFAAs), which structurally resemble biological fatty acids and have recently been associated with multiple endocrine disorders and soft tissue cancers.<sup>3–5</sup> This has led the United States Environmental Protection Agency (EPA) to impose strict PFAS treatment requirements for water municipalities to reduce exposure to the population. However, modern water and wastewater treatment practices are unable to adequately treat PFAS, allowing their bioaccumulation in aquatic ecosystems, plants, and surrounding populations.

Currently, the state-of-the-art method for removing PFAS from water is through adsorption onto granular activated carbon (GAC). GAC is commonly utilized in drinking water treatment trains to nonspecifically remove organics and

<sup>a</sup> Department of Biosystems Engineering, University of Arizona, Tucson, AZ 85721, USA

<sup>b</sup> Department of Chemical and Environmental Engineering, University of Arizona, Tucson, AZ 85721, USA. E-mail: vkaranik@arizona.edu; Tel: +1 (520) 621 5881

† Electronic supplementary information (ESI) available. See DOI: <https://doi.org/10.1039/d4lf00228h>



other odorous molecules. The sorption of PFAS onto GAC is dominated by both intraparticle diffusion and nonspecific hydrophobic and electrostatic interactions with the GAC surface active sites.<sup>6–8</sup> Longer-chained ( $C_n$ ,  $n > 6$ ) PFAS pose a greater potential to form aggregate structures, which can block GAC pore openings.<sup>9</sup> This can substantially reduce the surface area available for adsorption, and further result in premature breakthroughs. In addition, shorter-chained ( $C_n$ ,  $n \leq 6$ ) PFAS have displayed lower adsorption affinities to GAC due to their increased mobility, which permits rapid breakthrough of the sorbent bed, in comparison to their longer chained counterparts.<sup>10</sup> In each case the sorbent material needs to be replaced or regenerated before treatment can continue. However, when GAC is completely saturated with PFAS, it cannot be sustainably regenerated.<sup>11</sup> When PFAS adhere to GAC, the only effective regeneration is by subjecting the saturated mediums to temperatures that range between 800–1000 °C in a dry nitrogen environment.<sup>12</sup> The associated energy and operational costs of PFAS adsorption and regeneration with GAC forces utilities to landfill their spent sorbent and purchase new material when it comes time for replacement.<sup>13</sup> As such, investigating and understanding the mechanisms of PFAS adhesion to sorbent interfaces is essential to improving PFAS treatment practices.

The molecular interactions that generate PFAS adhesion at the solid–liquid interface are dynamic and complex. The specific makeup of the aqueous environment and surface composition directly impact the kinetics and extent of PFAS adsorption and adhesion.<sup>14</sup> The structure of the specific PFAS molecules in question also determine how they behave in the aqueous environment, as PFAS exist in multitudinous combinations of chain lengths and functional terminations.<sup>15</sup> The most common environmentally relevant PFAS molecules are aliphatic, with fluorocarbon chain lengths ranging between three to ten carbons and a charged terminal group of either carboxylate or sulfonate. The hydrophobic chain and hydrophilic functional group provide opportunities for PFAS to adsorb onto various matrices.<sup>16</sup> Therefore, it is widely accepted that PFAS adsorption will occur through hydrophobic and/or electrostatic attraction when a non-polar or polar adsorbent surface is present.<sup>17</sup> The development of optimized PFAS sorbents that have a selective affinity for PFAS compared to other co-solutes is predicated on tailoring molecular interactions for individual PFAS molecules.

Exploiting the properties of PFAS molecules to enhance their adsorption necessitates an understanding of molecular interactions that occur between PFAS and a sorbent in solution. The three primary interactions that drive PFAS adsorption and adhesion are electrostatic interactions, hydrophobic interactions, and Van der Waals forces that occur upon surface contact.<sup>18</sup> Each of these fundamental interactions can be manipulated by changing specific parameters in solution. Electrostatic forces in aqueous media are highly dependent on the ionic composition and strength, as introduction of charged species in solution will cause

particles to either attract or repel.<sup>19</sup> The hydrophobic effect is believed to be the result of excluded volume entropy change between non-polar molecules and water.<sup>20–22</sup> The magnitude of a molecule's hydrophobicity is dependent on its non-polar molar volume. There is currently no unified explanation of the origin of force exerted by hydrophobic interactions, but it is believed that it is not impacted by ionic strength alone, but rather by ionic species and solute size.<sup>23,24</sup> The degree of entropy or “order” of water has become a topic of interest in the study of hydrophobic interactions, as it can be affected by specific co-solutes. Specific ions and molecules have previously been labeled as kosmotropic, structure-making, or chaotropic, structure breaking.<sup>25</sup> Each has an opposite effect on neighboring water molecules and can be exploited for certain applications such as manipulating solubility, controlling ice nucleation, regulating micelle formation, and protein separation.<sup>26–30</sup> In the early 1940s, certain cations and anions were ranked according to their effect on water structure creating the Hofmeister scale.<sup>31</sup> It has been documented that specific ions in solution will have either a kosmotropic or chaotropic effect within a certain ion concentration range.<sup>32</sup> Outside this range however, their Hofmeister effect can be neutralized or reversed depending on the ionic species in question.<sup>33</sup> In addition to Hofmeister effects, Van der Waals interactions, particularly dipole–dipole interactions, can be affected by ionic strength and speciation. The fluorinated chains in PFAS molecules are conventionally described as non-polar because they demonstrate hydrophobic behavior due to their molecular geometry, but the possible impact of the polarity of the fluorocarbon backbone on Van der Waals interactions are seldom discussed. Only recently studies have begun to describe interactions with fluorocarbon molecules as polar–hydrophobic interactions.<sup>34–36</sup> The interplay of these dynamic forces arising from the combined surface, solute, and solvent chemistries determines the range and magnitude of adhesion a molecule experiences at an interface. This adhesion force can be measured using high resolution analytical techniques.

Force measurements taken with atomic force microscopy (AFM) have been utilized to approximate Van der Waals and hydrophobic interactions.<sup>37</sup> They can be conducted in solution, under dynamic conditions, and have been utilized for innumerable biological, material, and chemical experiments.<sup>38–40</sup> Only recently have studies begun to include force spectroscopy for measuring the adhesion forces of fluorinated contaminants for PFAS remediation applications. Mohona *et al.* probed the adhesion of bare AFM tips on self-assembled monolayers (SAMs) contaminated with PFOS and perfluorononanoic acid (PFNA), where they observed higher adhesion forces on PFAS contaminated surfaces compared to the control SAM.<sup>41</sup> Jin *et al.* measured the adhesion force between amyloid fibers in sampled lake water using PFOA and PFOS functionalized AFM tips and determined that adhesion was enhanced compared to unmodified tips.<sup>42</sup> While these pioneering experiments elucidate the fundamental behavior of PFAS at the solid–liquid interface,



AFM experiments can be used specifically to investigate the conditions for increasing and weakening PFAS adhesion.

In this study, the tunability of PFAS adhesion was examined by conducting adhesion force measurements with AFM using PFAS functionalized AFM tips on model surfaces representing classes of surface properties. Three silane molecules, aminopropyltriethoxysilane (APTES), triethoxy(octyl)silane (C8), and trimethoxy(octadecyl)silane (C18) were utilized to generate uniform siloxane thin films on silicon wafers. Surface modification of silicon wafers with different silanes allowed for polar and nonpolar interfaces to be obtained bearing specific physicochemical properties. These surfaces were then probed with a short and long chain PFAS – *e.g.*, perfluorobutanesulfonic acid (PFBS) and perfluorooctanesulfonate (PFOS) – to further characterize their adhesion force with the manufactured interfaces. All measurements were then repeated in electrolyte solutions – *e.g.*, 75 mM NaCl and 75 mM MgCl<sub>2</sub>. The impact of salt species and surface composition on adhesion was investigated for PFAS molecules, PFOS and PFBS, on three siloxane films.

## 2. Materials and methods

Mechanical grade silicon wafers with a diameter of 25.4 mm were purchased from University Wafer (South Boston, Massachusetts, U.S.). Silane molecules aminopropyltriethoxysilane (APTES), triethoxyoctylsilane (C8), and trimethoxyoctadecylsilane (C18) shown in Fig. 1, and (99%) magnesium chloride, and sodium chloride were purchased from Sigma Millipore (Burlington, Massachusetts, U.S.). (PFOA), 99% perfluorooctanesulfonic acid (PFOS), and 95% perfluorobutanesulfonic acid (PFBS) were also purchased from Sigma. Isotopically labeled standards for each mentioned PFAS molecule were purchased from Wellington Labs (Guelph, Ontario, Canada). HPLC grade (99%) methanol, ethanol, and hexane were purchased from VWR International (Randor, Pennsylvania, U.S.).



Fig. 1 Silane molecules aminopropyltriethoxysilane (APTES), triethoxy(octyl)silane (C8), and trimethoxy(octadecyl)silane (C18).

### 2.1. Surface preparation

All silicon wafers were cleaned and pretreated for five minutes with oxygen plasma using an Optiglow ACE plasma treatment unit (Tempe, AZ, U.S.). A plasma treated silicon wafer was prepared as a control sample. Each sample was subsequently submerged in a 1% solution of either polar (APTES) or nonpolar silane (C8 or C18) in ethanol or hexane respectively. Samples were allowed to react on a shaker plate at 60 rpm for 24 hours. Samples were subsequently rinsed and sonicated in their respective solvents for 15 minutes and dried gently with nitrogen. Samples were dried and cured in a vacuum oven at 100 °C for 1 hour prior to characterization.

### 2.2. Physical/chemical characterization

Contact angle measurements were taken with a Kruss Scientific DSA25E drop shape analyzer (Hamburg, Germany). Deionized water droplets of a 2  $\mu$ L volume were placed onto each sample and the mean contact angles were measured within five seconds. Ten replicates of each surface modification were used to generate an average value.

Streaming zeta potential of each siloxane film was determined with an Anton Paar Surpass 3 Streaming Zeta Potential (Graz, Austria). Silicon wafer samples were cut into 20 mm  $\times$  10 mm rectangles and affixed to the testing planes of the supplied gap cell. DI water was adjusted to the initial conductivity value of 15 millisiemens per centimeter (1 mM) required for operation with potassium chloride. Five zeta potential measurements were taken at each pH value ranging from 2 to 10 to create a pH dependence plot.

Streaming zeta potential measurements taken in sodium chloride and magnesium chloride solutions were conducted at different concentrations. Initial measurements were taken in deionized water prior to the addition of magnesium chloride. Magnesium chloride was added in 5 mL, 0.001 M increments until a final concentration of 0.1 M was reached. Streaming zeta potential measurements taken above 0.1 M salt concentrations became unreliable due to operational limitations of the instrument and were excluded from the analysis.<sup>43</sup>

The surface composition of the modified silicon wafers was analyzed *via* X-ray photoelectron spectroscopy analysis (XPS) using a Kratos Axis Ultra 165 Hybrid Photoelectron Spectrometer (Wharfside, Manchester, U.K.). Topographical information about the modified silicon surfaces was taken with atomic force microscopy (AFM) using the Nanosurf Cypher Atomic Force Microscope (Liestal, Switzerland). Modified silicon wafers were equilibrated in deionized water and scanned from ten points over a 1-micron area in contact mode with Aspire CT130 silicon nitride tips (Nanoscience Instruments, Tempe, AZ). The resulting data was processed with Gwyddion and zero-flattened to reduce image angling. The relative mean squared roughness and surface area of each surface were determined from the resulting topography.



### 2.3. Adhesion force measurement

Sulfonate PFAS terminated AFM tips were functionalized by first depositing a  $\sim 5$  nm thick gold layer on the tip surface with a Ladd-Hummer 6.2 sputter coater (Ladd Research, Williston, VT) and then immersing in 5 ppm solutions of their respective molecules for 1 minute. All tips were gently dried with nitrogen following any submersion events. The success and stability of PFAS functionalization was confirmed by scanning for F 1s peaks (687–689 eV) *via* XPS, shown in Fig. S1† before and after AFM experiments. Force measurements were collected with an Asylum Research Cypher Atomic Force Microscope (Oxfordshire, United Kingdom) operating in contact mode. Force curves were analyzed with Asylum Research 15 software by integrating the area under the force-distance curves. Three replicates of each siloxane film were analyzed with one hundred force measurements collected over a 1 square micron area per sample. Measurements for each PFAS-surface combination were conducted in 500  $\mu\text{L}$  volumes of DI water and solutions of 75 mM sodium chloride and 75 mM magnesium chloride.

## 3. Results and discussion

### 3.1. Characterization of model surfaces

Silicon wafers were modified with siloxane films to create model surfaces for PFAS adsorption. The surface properties of the deposited films were used to elucidate the impact of interfacial composition on PFAS adhesion. APTES represented a polar surface to investigate the impact of electrostatic interactions, while the eight carbon (C8) and 18 carbon (C18) silanes were chosen to examine the influence of hydrocarbon chain length and magnitude of hydrophobicity on PFAS adsorption.<sup>44,45</sup> A plasma treated sample containing no siloxane film was used as an unmodified reference for comparison of characterization results. The general reaction mechanism for the modification of silicon surfaces with silanes is shown in Fig. 2. Hydroxyl groups generated during plasma treatment act as nucleophiles and react with the suspended silane molecules, creating covalent bonds on the silicon surface and between other silane molecules. Fig. 3 depicts the measured water contact angles of the deposited siloxane films. The C8 and C18 samples were determined to

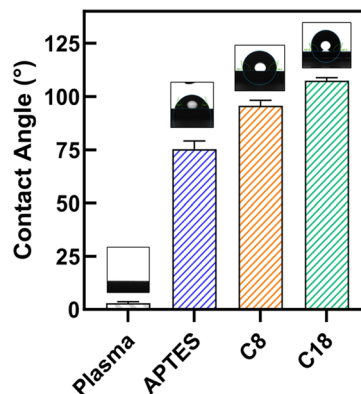


Fig. 3 Static contact angle measurements of modified silicon wafers taken with a 5  $\mu\text{L}$  water droplet immediately after contact.

be hydrophobic, having contact angles of  $104.52 (\pm 1.98)$  and  $109.87 (\pm 2.44)$ , respectively. The amine terminated and plasma treated samples were considered hydrophilic with contact angles significantly less than ninety degrees.

The topographical AFM scans shown in Fig. 4 and roughness data in Table S1† exhibited similar film morphologies and only slight variations in roughness between samples. The lower surface roughness of the C18 film surface compared to the more rigid C8 silane molecules suggests that the longer carbon chains fold over onto themselves in solution to minimize their contact with water molecules. XPS scans also shown in Fig. 5 indicated that the carbon content of each wafer increased; corresponding with the hydrocarbon chain lengths of each film. The nitrogen content of the APTES surface was approximately 2% and was not detected on the hydrophobic or plasma treated surfaces.

### 3.2. PFAS adhesion to siloxane films

To understand the electrostatic contribution to PFAS adhesion force, streaming zeta potential measurements were taken of each functionalized surface. The electrical double layer (EDL) is a combination of the region defined as the layer of adsorbed water molecules and ions on a surface called the stern layer, and the diffuse regime above the stern layer expanding to the electrostatic boundary of a surface deemed the slipping plane.<sup>46</sup> The zeta potential, the electrostatic potential measured at the outer boundary of the slipping plane, is widely utilized to estimate the general attraction or repulsion of molecules to a surface. The zeta potential exists due to acid-base reactions occurring on the material surface and adsorption of ions to the interface in solution.<sup>47</sup> Modulating or designing a surface to carry a specific zeta potential is a modern technique used for many applications including enhancing oil recovery from carbonate rock, rendering biomaterials inert to evade immune response, and separation and elution of polar molecules.<sup>48–50</sup> The isoelectric point (IEP), the pH at which a surface's zeta potential is equal to zero, is often used to obtain information about the functional behavior of the interface.<sup>51–53</sup> Fig. 6a

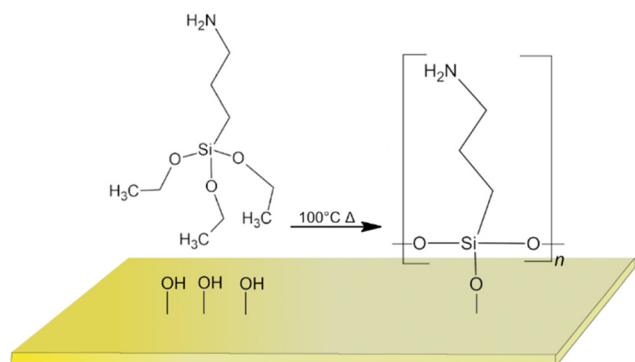


Fig. 2 APTES modification of a silicon.







Fig. 4 AFM topographical scans of each siloxane film. a) Plasma treated, b) APTES, c) C8, d) C18.

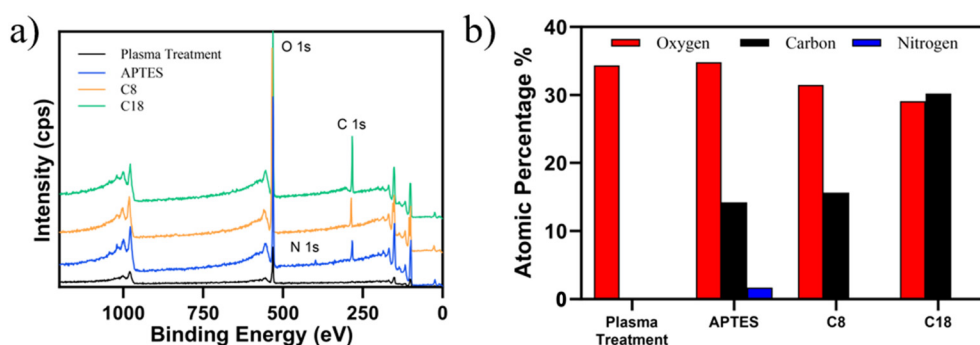


Fig. 5 (a) XPS spectra of each sample surface (b) atomic composition of each film surface.

shows the effect of pH titration on the zeta potential of each wafer sample from pH 2–10 in 1 mM potassium chloride. The APTES sample expectedly showed a basic surface functionality compared to acidic C8, and amphoteric C18. The high isoelectric point (pH 8) of APTES is in close agreement with pKa values and IEP data reported by Bhat *et al.* who modulated the sorption of nanoparticles by pH titration of an APTES modified silicon wafer.<sup>54</sup> The plasma treated control sample had an IEP of 5 and demonstrated amphoteric behavior, consistent with known pKa values and properties of silanols.<sup>55</sup> Examination of individual zeta potential values revealed that the APTES sample carried a positive electrostatic potential, the C8 surface was negative, and the C18 surface was at its isoelectric point at environmentally relevant pH of 6.8. Hydrophobic surfaces are expected to carry a negative zeta potential. At neutral pH values as water molecules are repelled from the interface, hydroxide ions are attracted to the positive dipoles on the

C–H chains that predominantly exist on the surface, generating a net negative electrostatic potential.<sup>56</sup> The lower magnitude of zeta potential and difference in isoelectric point of the C18 sample compared to C8 can be attributed to the longer carbon chain length. The folding over and charge condensation of the C18's longer carbon chains allows for the reduction in the net dipole moment of the molecule, reducing VdW interactions with hydroxide and thus resulting in a more positive surface potential and higher isoelectric point.<sup>43,57</sup> Though the C18 film is of comparable hydrophobicity to C8, the longer chains convey lower surface roughness and amphoteric behavior compared to the shorter chain modification.

Next, AFM was used to generate force curve profiles of PFOS and PFBS on the siloxane films in DI water. The baseline adhesion behavior of the polar-hydrophobic fluorocarbon chains in DI water is presented in Fig. 6b. PFAS molecules comprised of either four or eight carbons, and





Fig. 6 a) Plots of zeta potential versus pH for modified surfaces in 1 mM potassium chloride. b) Adhesion force measurements taken on modified surfaces in deionized water.

sulfonate head groups (PFOS and PFBS) were utilized to determine if fluorocarbon chain length or surface composition was the dominant contributor to the adhesion force. Unmodified AFM tips were not used as a control comparison in this study as previous experimentation yielded significant adhesion between the silicon nitride tip and amine terminated APTES functionalization. It is important to note that because the sulfonate groups were used to functionalize the molecules to the AFM tip, we hypothesize that the resulting force values would mostly correspond to the interaction between the exposed fluorocarbon tails and the substrates. Adhesion of both PFOS and PFBS was the weakest on the plasma treated surface. The high energy, hydrophilic surface of the plasma treated silicon wafer has little affinity for the hydrophobic PFAS tails. Of the surface modified samples, adhesion was lowest on the APTES film likely due to the excluded or inaccessible sulfonate groups, which minimize electrostatic attraction with the amine terminated surface. The negative dipoles of the fluorocarbon backbone, however, can interact with the amine groups, resulting in a Van der Waals adhesion force. The hydrophilicity of the APTES sample would also result in a lower hydrophobic interaction between the geometrically hydrophobic PFAS tails compared to the C8 and C18 surfaces. The PFBS functionalized tip had slightly higher adhesion on all surfaces (APTES: 129.21%, C8: 138.75%, C18: 161.52%) compared to PFOS. It is possible that the smaller molar volume and thus lower hydrophobicity of the fluorocarbon tail allows PFBS molecules to penetrate the adsorbed water layer more effectively on the sample surfaces.

Next, electrolyte solutions were introduced to examine how the presence of ions influence PFAS behavior at the interface. The specific behavior and magnitude of electrostatic interactions in the bulk solution and at the solid-liquid interface are impacted by the concentration of ions in solution.<sup>56,58</sup> This behavior was interpreted through additional zeta potential and force measurements in 75 mM NaCl, and 75 mM MgCl<sub>2</sub> solutions. Magnesium and sodium chloride were chosen as they are simple, low cost monovalent and divalent salts. Magnesium was selected over calcium chloride due to its smaller Van der Waals radius and ability

to impart a kosmotropic ordering effect with its tightly coordinated water molecules. A concentration of 75 mM was chosen as it is believed that ion concentrations greater than 10 mM are capable of generating Hofmeister effects.<sup>59</sup> Fig. 7 shows the zeta potential values at pH 6.8 ± 0.3 of each siloxane film and AFM tip functionalization in 1 mM KCl or 75 mM MgCl<sub>2</sub>. The AFM tip functionalizations carry positive zeta potentials in 1 mM KCl likely due to the attraction of hydronium ions to the negative dipoles on the fluorine atoms of the fluorocarbon tail. The shift towards negative zeta potential values in the presence of 75 mM magnesium chloride has been reported previously and is believed to be the result of the attraction of chloride and hydroxide ions to surface adsorbed magnesium ions.<sup>60</sup>

AFM adhesion force data are compiled for each surface-PFAS-solution combination in Fig. 8. Overall, the adhesion force of all PFAS molecules on each surface remained the lowest in deionized water. In deionized water, adsorbed water molecules on the film surface are at a maximum, potentially restricting access or lowering surface affinity to hydrophobic molecules.<sup>61</sup> Without ions in solution to adsorb to the film surface, the formation of a stable zeta potential and thus surface charge is not possible. The absence of ions also

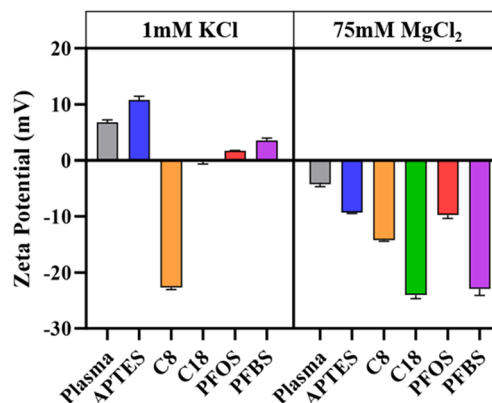


Fig. 7 Zeta potential measurements modified surfaces and AFM tip functionalizations taken in 1 mM potassium chloride and 75 mM magnesium chloride at pH 6.8.

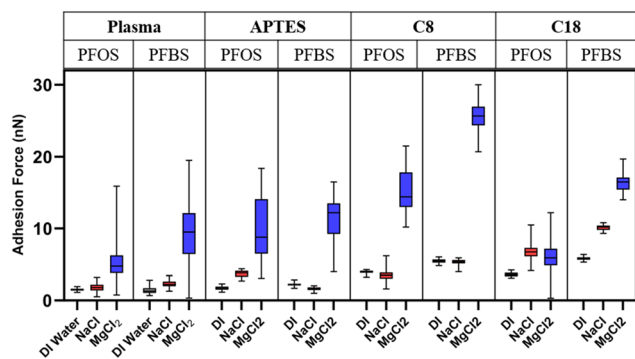


Fig. 8 Adhesion force boxplots of each modified surface-PFAS combination in 75 mM sodium chloride, 75 mM magnesium chloride.

prevents bridging of dipoles on the C-F backbones to the functionalized surfaces. In DI water there is no significant driving force for PFAS adhesion.

The addition of sodium chloride in solution provided a negligible impact on PFAS adhesion on the plasma treated, APTES, and C8 surfaces which corresponds to similar findings discussed in literature.<sup>62,63</sup> Sodium, compared to magnesium, has a lower charge density conveying a lower affinity for surfaces and molecules than magnesium. The C18 surface, however, showed a minor increase in adhesion force for both PFOS and PFBS in the 75 mM sodium chloride solution. In the presence of 75 mM  $\text{MgCl}_2$  the adhesion of PFOS and PFBS increased substantially on all surfaces. The increase in adhesion can be explained by several phenomena. The larger charge density and the water structuring effects of the magnesium ions compared to sodium creates a kosmotropic ordering effect.<sup>64</sup> Magnesium interacting with both tip and interfacial surface carry between 6 and 32 strongly coordinated water molecules in their hydration shells depending on ionic strength.<sup>46,65,66</sup> The increased structuring of the water hydrogen bonding network generated by magnesium ions creates a more pronounced Hofmeister effect resulting in greater expulsion of hydrophobic molecules from the bulk solution. This could also be responsible for enhancing PFAS sorption at the solid-liquid interface by structuring a hydrogen bonding network between tip and surface.<sup>67</sup>

Ion-dipole or cation bridging interactions arising from the addition of divalent magnesium ions may also contribute to the adhesion of PFAS chains at the interface. While the fluorocarbon backbone is geometrically non-polar, individual carbon-fluorine bonds have strong permanent dipoles ( $-1.43$  Debyes) that can interact with the magnesium ions and potentially bridge the C-F tails to the interface.<sup>68-70</sup> A recent study by Huang *et al.* has demonstrated that introducing sites for ion-dipole interactions on hydrophobic fluorocarbon polymers can increase their adhesion strength by 62%.<sup>71</sup> Divalent cations are also known for enhancing the partitioning of PFAS to solid-liquid and air-liquid interfaces.<sup>14,72-75</sup> The suggested mechanisms for which are charge suppression of anionic

PFAS headgroups that would be electrostatically repelled from negatively charged surfaces and cation bridging between PFAS and surfaces. Because only the PFAS tails are believed to be exposed in this study, cation bridging is the more likely explanation for the observed change in adhesion in this work.

The PFAS adhesion trends seen in Fig. 8 can also be described in terms of the polarizability of each film. The zeta potential data shown in Fig. 7 is in agreement with previous research that has concluded that the polarizability of alkyl molecules increases with carbon chain length.<sup>76,77</sup> It is also well understood that the strength of induced dipole interactions increases with increasing magnitude of zeta potential.<sup>78,79</sup> The PFAS adhesion patterns in Fig. 8 show that with increasing polarizability of probe-surface combination, a stronger adhesion force is generated. The C18 film, however, is an exception to this explanation as it has the highest zeta potential, and thus polarizability, but low adhesion force compared to other sample combinations. Because AFM measurements are physical in nature, the surface mechanical properties play a significant role. It is likely that because the C18 film is soft compared to the C8 and APTES films, during contact with the AFM tip, a mechanically stable interaction does not form. In addition, the C18 film had a roughness value lower than C8 and comparable to the plasma treated silicon wafer indicating again that possibly a layering or folding phenomenon may be at play. Further investigation into the influence of film viscoelastic properties is required to fully understand PFAS adhesion to complex film surfaces.

## 4. Conclusion

This study demonstrates the potential of utilizing cation solutions to manipulate PFAS adhesion. Examination of model surfaces composed of siloxane films yielded that adhesion of the PFAS fluorocarbon backbone can be enhanced with the addition of magnesium chloride. AFM force spectroscopy and zeta potential measurements revealed that the addition of 75 mM magnesium chloride provided the greatest enhancement to adhesion for both four and eight carbon PFAS on all sample surfaces. The proposed mechanism for the augmentation of PFAS adhesion is threefold. First, magnesium ions bind to the film surfaces and interact with the dipoles on the PFAS fluorocarbon tails, bridging the PFAS to the surface upon contact. Second, the addition of magnesium ions induces a kosmotropic ordering effect in the bulk solution, creating a higher energy water structure that enhances the hydrophobic effect. Lastly, the impact of magnesium on the zeta potential and thus polarizability of the film-tip interface increases the magnitude of induced dipole strength, enhancing Van der Waals forces upon contact. Additional research is necessary on the relationship between PFAS adhesion and adsorption with different co-solutes to gain a deeper understanding of how the sorption process can be further modulated.



## Data availability

Data for this article, including experimental logs are available at University of Arizona repository and stored in laboratory Google Drive files in Excel format. The data supporting this article have been included as part of the ESI.†

## Author contributions

J. Welchert: investigation, methodology, data curation, validation, writing – original draft, and visualization. M. Dunmyer: investigation, writing – reviewing & editing. L. Carroll: investigation. I. Martinez: investigation. T. Jean-Lane: investigation. D. Bellido-Aguilar: writing – review & editing. S. Savagatrup: writing – review & editing. V. Karanikola: supervision, project administration, funding acquisition, and writing – review & editing.

## Conflicts of interest

There are no conflicts of interest to declare.

## Acknowledgements

This work was made possible by the funding provided by the Arizona Board of Regents. We would also like to recognize Dr. Brooke Beam-Massani of the W.M. Keck Center for Nano-Scale Imaging and Paul Lee of the Laboratory of Electron Spectroscopy (LESSA) for their technical expertise and assistance.

## References

- 1 L. G. T. Gaines, Historical and current usage of per- and polyfluoroalkyl substances (PFAS): a literature review, *Am. J. Ind. Med.*, 2022, **66**, 353–378, DOI: [10.1002/ajim.23362](#).
- 2 M. Ateia, A. Alsbaiee, T. Karanfil and W. Dichtel, Efficient PFAS Removal by Amine-Functionalized Sorbents: Critical Review of the Current Literature, *Environ. Sci. Technol. Lett.*, 2019, **6**(12), 688–695, DOI: [10.1021/acs.estlett.9b00659](#).
- 3 A. J. Blomberg, L. S. Haug, C. Lindh, A. Sabaredzovic, D. Pineda, K. Jakobsson and C. Nielsen, Changes in Perfluoroalkyl Substances (PFAS) Concentrations in Human Milk over the Course of Lactation: A Study in Ronneby Mother-Child Cohort, *Environ. Res.*, 2023, **219**, 115096, DOI: [10.1016/j.envres.2022.115096](#).
- 4 N. Kotlarz, J. McCord, D. Collier, C. S. Lea, M. Strynar, A. B. Lindstrom, A. A. Wilkie, J. Y. Islam, K. Matney, P. Tarte, M. E. Polera, K. Burdette, J. DeWitt, K. May, R. C. Smart, D. R. U. Knappe and J. A. Hoppin, Measurement of Novel, Drinking Water-Associated PFAS in Blood from Adults and Children in Wilmington, North Carolina, *Environ. Health Perspect.*, 2020, **128**(7), 077005, DOI: [10.1289/EHP6837](#).
- 5 S. Cakmak, A. Lukina, S. Karthikeyan, E. Atlas and R. Dales, The Association between Blood PFAS Concentrations and Clinical Biochemical Measures of Organ Function and Metabolism in Participants of the Canadian Health Measures Survey (CHMS), *Sci. Total Environ.*, 2022, **827**, 153900, DOI: [10.1016/j.scitotenv.2022.153900](#).
- 6 X. Lei, Q. Lian, X. Zhang, T. K. Karsili, W. Holmes, Y. Chen, M. E. Zappi and D. D. Gang, A Review of PFAS Adsorption from Aqueous Solutions: Current Approaches, Engineering Applications, Challenges, and Opportunities, *Environ. Pollut.*, 2023, **321**, 121138, DOI: [10.1016/j.envpol.2023.121138](#).
- 7 M. Park, S. Wu, I. J. Lopez, J. Y. Chang, T. Karanfil and S. A. Snyder, Adsorption of Perfluoroalkyl Substances (PFAS) in Groundwater by Granular Activated Carbons: Roles of Hydrophobicity of PFAS and Carbon Characteristics, *Water Res.*, 2020, **170**, 115364, DOI: [10.1016/j.watres.2019.115364](#).
- 8 Q. Yu, R. Zhang, S. Deng, J. Huang and G. Yu, Sorption of Perfluorooctane Sulfonate and Perfluorooctanoate on Activated Carbons and Resin: Kinetic and Isotherm Study, *Water Res.*, 2009, **43**(4), 1150–1158, DOI: [10.1016/j.watres.2008.12.001](#).
- 9 D. Brown and A. LeBlanc, Navigating PFAS Treatment With GAC and Ion Exchange, *J. AWWA*, 2022, **114**(7), 36–43, DOI: [10.1002/awwa.1959](#).
- 10 E. R. Forrester, Removal of Short Chain PFAS via GAC Adsorption, *J. N. Engl. Water Works Assoc.*, 2019, **133**(2), 81–84.
- 11 E. Gagliano, M. Sgroi, P. P. Falciglia, F. G. A. Vagliasindi and P. Roccaro, Removal of Poly- and Perfluoroalkyl Substances (PFAS) from Water by Adsorption: Role of PFAS Chain Length, Effect of Organic Matter and Challenges in Adsorbent Regeneration, *Water Res.*, 2020, **171**, 115381, DOI: [10.1016/j.watres.2019.115381](#).
- 12 E. Gagliano, P. P. Falciglia, Y. Zaker, T. Karanfil and P. Roccaro, Microwave Regeneration of Granular Activated Carbon Saturated with PFAS, *Water Res.*, 2021, **198**, 117121, DOI: [10.1016/j.watres.2021.117121](#).
- 13 C. C. Murray, R. E. Marshall, C. J. Liu, H. Vatankhah and C. L. Bellona, PFAS Treatment with Granular Activated Carbon and Ion Exchange Resin: Comparing Chain Length, Empty Bed Contact Time, and Cost, *J. Water Process. Eng.*, 2021, **44**, 102342, DOI: [10.1016/j.jwpe.2021.102342](#).
- 14 M. L. Brusseau and S. Van Glubt, The Influence of Surfactant and Solution Composition on PFAS Adsorption at Fluid-Fluid Interfaces, *Water Res.*, 2019, **161**, 17–26, DOI: [10.1016/j.watres.2019.05.095](#).
- 15 X. Liu, X. Huang, X. Wei, Y. Zhi, S. Qian, W. Li, D. Yue and X. Wang, Occurrence and Removal of Per- and Polyfluoroalkyl Substances (PFAS) in Leachates from Incineration Plants: A Full-Scale Study, *Chemosphere*, 2023, **313**, 137456, DOI: [10.1016/j.chemosphere.2022.137456](#).
- 16 M. L. Brusseau, The Influence of Molecular Structure on the Adsorption of PFAS to Fluid-Fluid Interfaces: Using QSPR to Predict Interfacial Adsorption Coefficients, *Water Res.*, 2019, **152**, 148–158, DOI: [10.1016/j.watres.2018.12.057](#).
- 17 X. Liu, C. Zhu, J. Yin, J. Li, Z. Zhang, J. Li, F. Shui, Z. You, Z. Shi, B. Li, X.-H. Bu, A. Nafady and S. Ma, Installation of Synergistic Binding Sites onto Porous Organic Polymers for Efficient Removal of Perfluorooctanoic Acid, *Nat. Commun.*, 2022, **13**(1), 2132, DOI: [10.1038/s41467-022-29816-1](#).





- 18 S. Kancharla, P. Alexandridis and M. Tsianou, Sequestration of Per- and Polyfluoroalkyl Substances (PFAS) by Adsorption: Surfactant and Surface Aspects, *Curr. Opin. Colloid Interface Sci.*, 2022, **58**, 101571, DOI: [10.1016/j.cocis.2022.101571](https://doi.org/10.1016/j.cocis.2022.101571).
- 19 S. Chen, H. Dong and J. Yang, Surface Potential/Charge Sensing Techniques and Applications, *Sensors*, 2020, **20**(6), 1690, DOI: [10.3390/s20061690](https://doi.org/10.3390/s20061690).
- 20 R.-H. Yoon, D. H. Flinn and Y. I. Rabinovich, Hydrophobic Interactions between Dissimilar Surfaces, *J. Colloid Interface Sci.*, 1997, **185**(2), 363–370, DOI: [10.1006/jcis.1996.4583](https://doi.org/10.1006/jcis.1996.4583).
- 21 E. E. Meyer, K. J. Rosenberg and J. Israelachvili, Recent Progress in Understanding Hydrophobic Interactions, *Proc. Natl. Acad. Sci.*, 2006, **103**(43), 15739–15746, DOI: [10.1073/pnas.0606422103](https://doi.org/10.1073/pnas.0606422103).
- 22 F. Biedermann, W. M. Nau and H.-J. Schneider, The Hydrophobic Effect Revisited-Studies with Supramolecular Complexes Imply High-Energy Water as a Noncovalent Driving Force, *Angew. Chem., Int. Ed.*, 2014, **53**(42), 11158–11171, DOI: [10.1002/anie.201310958](https://doi.org/10.1002/anie.201310958).
- 23 Q. Sun, X. W. Su and C. B. Cheng, The Dependence of Hydrophobic Interactions on Solute Size, *Chem. Phys.*, 2019, **516**(2018), 199–205, DOI: [10.1016/j.chemphys.2018.09.014](https://doi.org/10.1016/j.chemphys.2018.09.014).
- 24 J. W. Kurutz and S. Xu, Hofmeister Solute Effects on Hydrophobic Adhesion Forces in SFM Experiments, *Langmuir*, 2001, **17**(23), 7323–7326, DOI: [10.1021/la010645s](https://doi.org/10.1021/la010645s).
- 25 S. Moelbert, B. Normand and P. De Los Rios, Kosmotropes and Chaotropes: Modelling Preferential Exclusion, Binding and Aggregate Stability, *Biophys. Chem.*, 2004, **112**(1), 45–57, DOI: [10.1016/j.bpc.2004.06.012](https://doi.org/10.1016/j.bpc.2004.06.012).
- 26 N. Vlachy, M. Drechsler, D. Touraud and W. Kunz, Anion Specificity Influencing Morphology in Catanionic Surfactant Mixtures with an Excess of Cationic Surfactant, *C. R. Chim.*, 2009, **12**(1), 30–37, DOI: [10.1016/j.crci.2008.10.010](https://doi.org/10.1016/j.crci.2008.10.010).
- 27 W. Kunz, Specific Ion Effects in Colloidal and Biological Systems, *Curr. Opin. Colloid Interface Sci.*, 2010, **15**(1), 34–39, DOI: [10.1016/j.cocis.2009.11.008](https://doi.org/10.1016/j.cocis.2009.11.008).
- 28 S. Wu, C. Zhu, Z. He, H. Xue, Q. Fan, Y. Song, J. S. Francisco, X. C. Zeng and J. Wang, Ion-Specific Ice Recrystallization Provides a Facile Approach for the Fabrication of Porous Materials, *Nat. Commun.*, 2017, **8**(1), 15154, DOI: [10.1038/ncomms15154](https://doi.org/10.1038/ncomms15154).
- 29 B. W. Ninham and V. Yaminsky, Ion Binding and Ion Specificity: The Hofmeister Effect and Onsager and Lifshitz Theories, *Langmuir*, 1997, **13**(7), 2097–2108, DOI: [10.1021/la960974y](https://doi.org/10.1021/la960974y).
- 30 J. Liu, C. Zhu, K. Liu, Y. Jiang, Y. Song, J. S. Francisco, X. C. Zeng and J. Wang, Distinct Ice Patterns on Solid Surfaces with Various Wettabilities, *Proc. Natl. Acad. Sci.*, 2017, **114**(43), 11285–11290, DOI: [10.1073/pnas.1712829114](https://doi.org/10.1073/pnas.1712829114).
- 31 Z. Yang, Hofmeister Effects: An Explanation for the Impact of Ionic Liquids on Biocatalysis, *J. Biotechnol.*, 2009, **144**(1), 12–22, DOI: [10.1016/j.jbiotec.2009.04.011](https://doi.org/10.1016/j.jbiotec.2009.04.011).
- 32 K. P. Gregory, G. R. Elliott, H. Robertson, A. Kumar, E. J. Wanless, G. B. Webber, V. S. J. Craig, G. G. Andersson and A. J. Page, Understanding Specific Ion Effects and the Hofmeister Series, *Phys. Chem. Chem. Phys.*, 2022, **24**(21), 12682–12718, DOI: [10.1039/D2CP00847E](https://doi.org/10.1039/D2CP00847E).
- 33 P. Luo, Y. Zhai, E. Senses, E. Mamontov, G. Xu, Y. Z and A. Faraone, Influence of Kosmotrope and Chaotrope Salts on Water Structural Relaxation, *J. Phys. Chem. Lett.*, 2020, **11**(21), 8970–8975, DOI: [10.1021/acs.jpclett.0c02619](https://doi.org/10.1021/acs.jpclett.0c02619).
- 34 J. C. Biffinger, H. W. Kim and S. G. DiMaggio, The Polar Hydrophobicity of Fluorinated Compounds, *ChemBioChem*, 2004, **5**(5), 622–627, DOI: [10.1002/cbic.200300910](https://doi.org/10.1002/cbic.200300910).
- 35 V. H. Dalvi and P. J. Rossky, Molecular Origins of Fluorocarbon Hydrophobicity, *Proc. Natl. Acad. Sci.*, 2010, **107**(31), 13603–13607, DOI: [10.1073/pnas.0915169107](https://doi.org/10.1073/pnas.0915169107).
- 36 L. Mayrhofer, G. Moras, N. Mulakaluri, S. Rajagopalan, P. A. Stevens and M. Moseler, Fluorine-Terminated Diamond Surfaces as Dense Dipole Lattices: The Electrostatic Origin of Polar Hydrophobicity, *J. Am. Chem. Soc.*, 2016, **138**(12), 4018–4028, DOI: [10.1021/jacs.5b04073](https://doi.org/10.1021/jacs.5b04073).
- 37 H.-J. Butt, B. Cappella and M. Kappl, Force Measurements with the Atomic Force Microscope: Technique Interpretation and Applications, *Surf. Sci. Rep.*, 2005, **59**(1–6), 1–152, DOI: [10.1016/j.surfrep.2005.08.003](https://doi.org/10.1016/j.surfrep.2005.08.003).
- 38 C. Aubry, L. Gutierrez and J. P. Croue, Coating of AFM Probes with Aquatic Humic and Non-Humic NOM to Study Their Adhesion Properties, *Water Res.*, 2013, **47**(9), 3109–3119, DOI: [10.1016/j.watres.2013.03.023](https://doi.org/10.1016/j.watres.2013.03.023).
- 39 M. Geisler, T. Pirzer, C. Ackerschott, S. Lud, J. Garrido, T. Scheibel and T. Hugel, Hydrophobic and Hofmeister Effects on the Adhesion of Spider Silk Proteins onto Solid Substrates: An AFM-Based Single-Molecule Study, *Langmuir*, 2008, **24**(4), 1350–1355, DOI: [10.1021/la702341j](https://doi.org/10.1021/la702341j).
- 40 P. Heidari, M. Salehi, B. Ruhani, V. Purcar and S. Căprărescu, Influence of Thin Film Deposition on AFM Cantilever Tips in Adhesion and Young's Modulus of MEMS Surfaces, *Materials*, 2022, **15**(6), 2102, DOI: [10.3390/ma15062102](https://doi.org/10.3390/ma15062102).
- 41 T. M. Mohona, Z. Ye, N. Dai and P. C. Nalam, Adsorption Behavior of Long-Chain Perfluoroalkyl Substances on Hydrophobic Surface: A Combined Molecular Characterization and Simulation Study, *Water Res.*, 2023, **239**, 120074, DOI: [10.1016/j.watres.2023.120074](https://doi.org/10.1016/j.watres.2023.120074).
- 42 T. Jin, M. Peydayesh, H. Joerss, J. Zhou, S. Bolisetty and R. Mezzenga, Amyloid Fibril-Based Membranes for PFAS Removal from Water, *Environ. Sci.: Water Res. Technol.*, 2021, **7**(10), 1873–1884, DOI: [10.1039/D1EW00373A](https://doi.org/10.1039/D1EW00373A).
- 43 T. Luxbacher, *The ZETA Guide: Principles of the Streaming Potential Technique*, Anton Paar GmbH, Graz, Austria, 2014.
- 44 J. Kim, P. Seidler, L. S. Wan and C. Fill, Formation, Structure, and Reactivity of Amino-Terminated Organic Films on Silicon Substrates, *J. Colloid Interface Sci.*, 2009, **329**(1), 114–119, DOI: [10.1016/j.jcis.2008.09.031](https://doi.org/10.1016/j.jcis.2008.09.031).
- 45 Y. Lu, Y. Wang, L. Liu and W. Yuan, Environmental-Friendly and Magnetic/Silanized Ethyl Cellulose Sponges as Effective and Recyclable Oil-Absorption Materials, *Carbohydr. Polym.*, 2017, **173**, 422–430, DOI: [10.1016/j.carbpol.2017.06.009](https://doi.org/10.1016/j.carbpol.2017.06.009).
- 46 X. Liu, R. Tian, R. Li, W. Ding, H. Li and R. Yuan, Principles for the Determination of the Surface Potential of Charged



- Particles in Mixed Electrolyte Solutions, *Proc. R. Soc. A*, 2015, **471**(2180), 20150064, DOI: [10.1098/rspa.2015.0064](https://doi.org/10.1098/rspa.2015.0064).
- 47 W. B. S. de Lint, N. E. Benes, J. Lyklema, H. J. M. Bouwmeester, A. J. van der Linde and M. Wessling, Ion Adsorption Parameters Determined from Zeta Potential and Titration Data for a  $\gamma$ -Alumina Nanofiltration Membrane, *Langmuir*, 2003, **19**(14), 5861–5868, DOI: [10.1021/la026864a](https://doi.org/10.1021/la026864a).
  - 48 N. Singh, P. H. Gopani, H. K. Sarma, P. Matthey, D. S. Negi, V. R. Srivastava and T. Luxbacher, Charging Behaviour at the Carbonate Rock-Water Interface in Low-Salinity Waterflooding: Estimation of Zeta Potential in High-Salinity Brines, *Can. J. Chem. Eng.*, 2022, **100**(6), 1226–1234, DOI: [10.1002/cjce.24311](https://doi.org/10.1002/cjce.24311).
  - 49 R. Zangi and B. J. Berne, Aggregation and Dispersion of Small Hydrophobic Particles in Aqueous Electrolyte Solutions, *J. Phys. Chem. B*, 2006, **110**(45), 22736–22741, DOI: [10.1021/jp064475+](https://doi.org/10.1021/jp064475+).
  - 50 B. Salopek, D. Krasi and S. Filipovi, MEASUREMENT AND APPLICATION OF ZETA-POTENTIAL, *Rud.-Geol.-Naftni Zb.*, 1992, **4**, 147–151.
  - 51 B. Zhu, P. Xia, W. Ho and J. Yu, Isoelectric Point and Adsorption Activity of Porous G-C<sub>3</sub>N<sub>4</sub>, *Appl. Surf. Sci.*, 2015, **344**, 188–195, DOI: [10.1016/j.apsusc.2015.03.086](https://doi.org/10.1016/j.apsusc.2015.03.086).
  - 52 Y.-F. Wu, W. Liu, N.-Y. Gao and T. Tao, A Study of Titanium Sulfate Flocculation for Water Treatment, *Water Res.*, 2011, **45**(12), 3704–3711, DOI: [10.1016/j.watres.2011.04.023](https://doi.org/10.1016/j.watres.2011.04.023).
  - 53 E. A. López-Maldonado, M. T. Oropeza-Guzman, J. L. Jurado-Baizaval and A. Ochoa-Terán, Coagulation–Flocculation Mechanisms in Wastewater Treatment Plants through Zeta Potential Measurements, *J. Hazard. Mater.*, 2014, **279**, 1–10, DOI: [10.1016/j.jhazmat.2014.06.025](https://doi.org/10.1016/j.jhazmat.2014.06.025).
  - 54 R. R. Bhat and J. Genzer, Tuning the Number Density of Nanoparticles by Multivariant Tailoring of Attachment Points on Flat Substrates, *Nanotechnology*, 2006, **18**(2), 025301, DOI: [10.1088/0957-4484/18/2/025301](https://doi.org/10.1088/0957-4484/18/2/025301).
  - 55 M. Sulpizi, M.-P. Gaigeot and M. Sprik, The Silica–Water Interface: How the Silanols Determine the Surface Acidity and Modulate the Water Properties, *J. Chem. Theory Comput.*, 2012, **8**(3), 1037–1047, DOI: [10.1021/ct2007154](https://doi.org/10.1021/ct2007154).
  - 56 M. Předota, M. L. Machesky and D. J. Wesolowski, Molecular Origins of the Zeta Potential, *Langmuir*, 2016, **32**(40), 10189–10198, DOI: [10.1021/acs.langmuir.6b02493](https://doi.org/10.1021/acs.langmuir.6b02493).
  - 57 M. N. Vo, M. Call, C. Kowall and J. K. Johnson, Effect of Chain Length on the Dipole Moment of Polyisobutylene Succinate Anhydride, *Ind. Eng. Chem. Res.*, 2022, **61**(5), 2359–2365, DOI: [10.1021/acs.iecr.1c03478](https://doi.org/10.1021/acs.iecr.1c03478).
  - 58 M. Takeya, M. Shimokawara, Y. Elakneswaran, T. Nawa and S. Takahashi, Predicting the Electrokinetic Properties of the Crude Oil/Brine Interface for Enhanced Oil Recovery in Low Salinity Water Flooding, *Fuel*, 2019, **235**, 822–831, DOI: [10.1016/j.fuel.2018.08.079](https://doi.org/10.1016/j.fuel.2018.08.079).
  - 59 Y. Marcus, Effect of Ions on the Structure of Water: Structure Making and Breaking, *Chem. Rev.*, 2009, **109**(3), 1346–1370, DOI: [10.1021/cr8003828](https://doi.org/10.1021/cr8003828).
  - 60 A. Alroudhan, J. Vinogradov and M. D. Jackson, Zeta Potential of Intact Natural Limestone: Impact of Potential-Determining Ions Ca, Mg and SO<sub>4</sub>, *Colloids Surf., A*, 2016, **493**, 83–98, DOI: [10.1016/j.colsurfa.2015.11.068](https://doi.org/10.1016/j.colsurfa.2015.11.068).
  - 61 Z. Zhang, S. Ryu, Y. Ahn and J. Jang, Molecular Features of Hydration Layers Probed by Atomic Force Microscopy, *Phys. Chem. Chem. Phys.*, 2018, **20**(48), 30492–30501, DOI: [10.1039/C8CP06126B](https://doi.org/10.1039/C8CP06126B).
  - 62 M. Bogunia and M. Makowski, Influence of Ionic Strength on Hydrophobic Interactions in Water: Dependence on Solute Size and Shape, *J. Phys. Chem. B*, 2020, **124**(46), 10326–10336, DOI: [10.1021/acs.jpcc.0c06399](https://doi.org/10.1021/acs.jpcc.0c06399).
  - 63 P. Amani and M. Firouzi, Effect of Divalent and Monovalent Salts on Interfacial Dilational Rheology of Sodium Dodecylbenzene Sulfonate Solutions, *Colloids Interfaces*, 2022, **6**(3), 41, DOI: [10.3390/colloids6030041](https://doi.org/10.3390/colloids6030041).
  - 64 R. Zangi, M. Hagen and B. J. Berne, Effect of Ions on the Hydrophobic Interaction between Two Plates, *J. Am. Chem. Soc.*, 2007, **129**(15), 4678–4686, DOI: [10.1021/ja068305m](https://doi.org/10.1021/ja068305m).
  - 65 M. Mahmoudvand, A. Javadi and P. Pourafshary, Brine Ions Impacts on Water–Oil Dynamic Interfacial Properties Considering Asphaltene and Maltene Constituents, *Colloids Surf., A*, 2019, **579**, 123665, DOI: [10.1016/j.colsurfa.2019.123665](https://doi.org/10.1016/j.colsurfa.2019.123665).
  - 66 G.-Z. Jia, S. Liu, F.-H. Liu and J.-C. Liu, Ion–Water Cooperative Interactions in Aqueous Solutions of MgCl<sub>2</sub> by Dielectric Spectroscopy, *J. Dispersion Sci. Technol.*, 2016, **37**(1), 1–5, DOI: [10.1080/01932691.2015.1010728](https://doi.org/10.1080/01932691.2015.1010728).
  - 67 X. Liu, H. Li, W. Du, R. Tian, R. Li and X. Jiang, Hofmeister Effects on Cation Exchange Equilibrium: Quantification of Ion Exchange Selectivity, *J. Phys. Chem. C*, 2013, **117**(12), 6245–6251, DOI: [10.1021/jp312682u](https://doi.org/10.1021/jp312682u).
  - 68 J. N. Israelachvili, Interactions Involving Polar Molecules. In *Intermolecular and Surface Forces*, Elsevier, 2011, pp. 71–90, DOI: [10.1016/B978-0-12-375182-9.10004-1](https://doi.org/10.1016/B978-0-12-375182-9.10004-1).
  - 69 Ş. Erkoç and F. Erkoç, Structural and Electronic Properties of PFOS and LiPFOS, *J. Mol. Struct.*, 2001, **549**(3), 289–293, DOI: [10.1016/S0166-1280\(01\)00553-X](https://doi.org/10.1016/S0166-1280(01)00553-X).
  - 70 R. L. Scott, The Anomalous Behavior of Fluorocarbon Solutions, *J. Phys. Chem.*, 1958, **62**(2), 136–145, DOI: [10.1021/j150560a002](https://doi.org/10.1021/j150560a002).
  - 71 S. Huang, Y. Wan, X. Ming, J. Zhou, M. Zhou, H. Chen, Q. Zhang and S. Zhu, Adhering Low Surface Energy Materials without Surface Pretreatment via Ion–Dipole Interactions, *ACS Appl. Mater. Interfaces*, 2021, **13**(34), 41112–41119, DOI: [10.1021/acsami.1c11822](https://doi.org/10.1021/acsami.1c11822).
  - 72 W. Cai, D. A. Navarro, J. Du, G. Ying, B. Yang, M. J. McLaughlin and R. S. Kookana, Increasing Ionic Strength and Valency of Cations Enhance Sorption through Hydrophobic Interactions of PFAS with Soil Surfaces, *Sci. Total Environ.*, 2022, **817**, 152975, DOI: [10.1016/j.scitotenv.2022.152975](https://doi.org/10.1016/j.scitotenv.2022.152975).
  - 73 R. Wu, X. Li, Y. Sun, P. Szymczak and W. Jiao, Second-Order Accurate Implicit Finite Volume Method for Two-Dimensional Modeling of PFAS Transport in Unsaturated Porous Media with Variable Surface Tension, *Adv. Water Resour.*, 2023, **178**, 104490, DOI: [10.1016/j.advwatres.2023.104490](https://doi.org/10.1016/j.advwatres.2023.104490).



- 74 S.-T. Le, Y. Gao, T. C. G. Kibbey, W. C. Glamore and D. M. O'Carroll, Predicting the Impact of Salt Mixtures on the Air-Water Interfacial Behavior of PFAS, *Sci. Total Environ.*, 2022, **819**, 151987, DOI: [10.1016/j.scitotenv.2021.151987](https://doi.org/10.1016/j.scitotenv.2021.151987).
- 75 C. You, C. Jia and G. Pan, Effect of Salinity and Sediment Characteristics on the Sorption and Desorption of Perfluorooctane Sulfonate at Sediment-Water Interface, *Environ. Pollut.*, 2010, **158**(5), 1343–1347, DOI: [10.1016/j.envpol.2010.01.009](https://doi.org/10.1016/j.envpol.2010.01.009).
- 76 J. A. Beran and L. Kevan, Semiempirical Calculation of Molecular Polarizabilities and Diamagnetic Susceptibilities of Fluorocarbons, Substituted Fluorocarbons, Ethers, Esters, Ketones, and Aldehydes, *J. Phys. Chem.*, 1969, **73**(11), 3860–3866, DOI: [10.1021/j100845a049](https://doi.org/10.1021/j100845a049).
- 77 M. Bianchetti, P. F. Buonsante, F. Ginelli, H. E. Roman, R. A. Broglia and F. Alasia, Ab-Initio Study of the Electromagnetic Response and Polarizability Properties of Carbon Chains, *Phys. Rep.*, 2002, **357**(6), 459–513, DOI: [10.1016/S0370-1573\(01\)00059-X](https://doi.org/10.1016/S0370-1573(01)00059-X).
- 78 H. Zhou, M. A. Preston, R. D. Tilton and L. R. White, Calculation of the Electric Polarizability of a Charged Spherical Dielectric Particle by the Theory of Colloidal Electrokinetics, *J. Colloid Interface Sci.*, 2005, **285**(2), 845–856, DOI: [10.1016/j.jcis.2004.11.065](https://doi.org/10.1016/j.jcis.2004.11.065).
- 79 G. M. Sacha, A. Verdaguer and M. Salmeron, A Model for the Characterization of the Polarizability of Thin Films Independently of the Thickness of the Film, *J. Phys. Chem. B*, 2018, **122**(2), 904–909, DOI: [10.1021/acs.jpcc.7b06975](https://doi.org/10.1021/acs.jpcc.7b06975).

